Радиофотоника

УДК 681.785.52 Научная статья

https://doi.org/10.32603/1993-8985-2025-28-5-66-82

Портативная многоспектральная камера для экологического мониторинга

В. С. Горяинов[1✉], Ж. Б. Нгуа Ндонг Авеле[1], А. Б. Мазоя[2], С. А. Тарасов[1]

[1] Санкт-Петербургский государственный электротехнический университет "ЛЭТИ" им. В. И. Ульянова (Ленина), Санкт-Петербург, Россия

[2]Университет Додомы, Додома, Танзания

✉ vsgoriainov@etu.ru

Аннотация

Введение. Пройдя длительный путь развития, пассивные спектральные методики дистанционного зондирования стали основным источником информации о состоянии земной поверхности и атмосферы. Многоспектральные и гиперспектральные камеры в настоящее время производятся серийно, однако их более широкому применению по-прежнему мешает высокая цена. Доступные в продаже дешевые фотоприемные CMOS-матрицы обеспечивают подходящую основу для разработки недорогих многоспектральных камер.

Цель работы. Создание переносной многоспектральной камеры, предназначенной для экологического мониторинга в полевых условиях.

Материалы и методы. Конструкция камеры основана на одной фотоприемной CMOS-матрице. Участки спектра выбираются сменяемыми интерференционными фильтрами, установленными в двух зубчатых колесах. Оптическая система камеры формирует параллельный пучок света перед его прохождением через фильтр, а затем фокусирует его в плоскости фотоприемной матрицы. Переключение фильтров обеспечивается шаговым электродвигателем. Его вращением, а также получением и сохранением изображений управляет одноплатный компьютер Raspberry Pi. Обработка многоспектральных изображений выполнялась при помощи программ на языке Python.

Результаты. Проведены испытания оптической схемы разработанной камеры для оценки размера и спектральной однородности ее поля зрения. Кроме того, с использованием камеры получены изображения растительности и рассчитаны пространственные распределения двух вегетационных индексов: нормализованного разностного вегетационного индекса (NDVI) и зелено-красного вегетационного индекса (GRVI). При помощи этих индексов удалось выделить на снимках области, занятые растительностью, а также отделить хвойные деревья от лиственных.

Заключение. Результаты испытаний показали применимость использованной оптико-механической схемы для удаленной оценки экологического состояния растительности.

Ключевые слова: многоспектральная съемка, недорогие научные приборы, фотоприемные матрицы CMOS, интерференционные фильтры, вегетационные индексы

Для цитирования: Портативная многоспектральная камера для экологического мониторинга / В. С. Горяинов, Ж. Б. Нгуа Ндонг Авеле, А. Б. Мазоя, С. А. Тарасов // Изв. вузов России. Радиоэлектроника. 2025. Т. 28, № 5. С. 66–82. doi: 10.32603/1993-8985-2025-28-5-66-82

Конфликт интересов. Авторы заявляют об отсутствии конфликта интересов.

Источник финансирования. Исследование выполнено в рамках проекта FSEE-2025-0013, выполнявшегося в рамках государственного задания Министерства науки и высшего образования Российской Федерации.

Статья поступила в редакцию 05.08.2025; принята к публикации после рецензирования 22.10.2025; опубликована онлайн 28.11.2025

Microwave Photonics

Original article

Portable Multispectral Camera for Environmental Monitoring

Viktor S. Goryainov[1✉], Jacques B. Ngoua Ndong Avele[1], Adam B. Mazoya[2], Sergey A. Tarasov[1]

[1]Saint Petersburg Electrotechnical University, Saint Petersburg, Russia
[2]University of Dodoma, Dodoma, Tanzania

✉ vsgoriainov@etu.ru

Abstract
Introduction. Passive spectral remote sensing techniques have come a long way to become the main source of information on the Earth's surface and atmosphere. Multispectral and hyperspectral cameras are now produced on a mass scale; however, their wider use is still impeded by high cost. Commercially available affordable complementary metal–oxide semiconductor (CMOS) image sensors provide a suitable basis for the development of low-cost multispectral cameras.
Aim. To design and test a portable multispectral camera intended for environmental monitoring in the field.
Materials and methods. The camera design is based on a single CMOS image sensor. Spectral bands are selected by interchangeable interference filters installed in two gear wheels. The optical system of the camera forms a parallel beam of light before its passing through a filter followed by focusing in the sensor plane. Filter switching is performed by a stepping motor. Its rotation, as well as image acquisition and storage, is controlled by a Raspberry Pi single-board computer. Multispectral images were processed using scripts in the Python language.
Results. The optical design of the newly created camera was tested to assess the size and spectral uniformity of its field of view. In addition, the camera was used to obtain several images of vegetation cover. Further, spatial distributions of two vegetation indices – the normalized difference vegetation index (NDVI) and the green–red vegetation index (GRVI) – were calculated. These distributions allowed areas occupied by vegetation to be successfully detected and coniferous trees to be separated from deciduous ones.
Conclusion. The results obtained have confirmed the feasibility of the proposed optical and mechanical design for remote assessment of the ecological status of vegetation cover.

Keywords: multispectral imaging, low-cost instrumentation, CMOS image sensors, interference filters, vegetation indices

For citation: Goryainov V. S., Ngoua Ndong Avele J. B., Mazoya A. B., Tarasov S. A. Portable Multispectral Camera for Environmental Monitoring. Journal of the Russian Universities. Radioelectronics. 2025, vol. 28, no. 5, pp. 66–82.
doi: 10.32603/1993-8985-2025-28-5-66-82

Conflict of interest. The authors declare no conflicts of interest.

Source of funding. The study was carried out as part of project FSEE-2025-0013, which was carried out as part of the state task of the Ministry of Science and Higher Education of the Russian Federation.

Submitted 05.08.2025; accepted 22.10.2025; published online 28.11.2025

Introduction. Passive imaging multispectral and hyperspectral devices have come a long way of development to become the main source of data in weather prediction and climatology, oceanology, agriculture, forestry, land use and land change monitoring, military reconnaissance. Initial experiments in airborne spectral remote sensing of natural objects were undertaken between 1910s and 1930s [1], with a practical goal of enhancing the quality of aerial photography by selecting proper spectral filters and film types.

At the beginning of the 1970s, when duration of space missions had extended to tens of days, spectral instruments began to increasingly find application in remote sensing experiments. In response to the growing demand for quantitative measurements, the technique of space spectrophotometry of the natural environment was developed based on the theoretical framework of classical photometry, including its calculation methods and empirical approaches to measuring radiative energy [2].

Some of the earliest spaceborne spectral devices, such as RSS portable spectrometers, were non-imaging [3]. Other types of devices relied on either obtaining images simultaneously by several co-directed cameras, each using a different band-pass optical filter [4], or using a single-element or multi-element photodetector possibly in combination with a mechanical system for spectral scanning [5]. Apart from manned space stations, scanning photoelectric spectrometers were concurrently installed on automatic remote sensing satellites, such as Landsat and Meteor-Priroda.

In the early 1980s, the term "hyperspectral imaging" was proposed by Alexander Goetz et al. (NASA Jet Propulsion Laboratory), emphasizing originally the ability to obtain a contiguous spectrum for each element in the image, rather than handling hundreds of narrow spectral bands [6]. While multispectral devices generally worked in atmospheric windows of low absorption, a contiguous spectrum was presumed to contain sufficient information to exclude the atmospheric influence from the measurement result [7].

The first airborne hyperspectral imager, referred to as the Airborne Imaging Spectrometer (AIS), employed a two-dimensional array (32 × 32 elements) of HgCdTe photodetectors bonded to a silicon CCD array. Together with the specific optical design of the instrument, this allowed obtaining images in 128 bands between 1.2 and 2.4 μm, with a spectral resolution of 9.6 nm [8]. In the following two decades, a number of hyperspectral instruments (AVIRIS, DAIS, CASI, HYDICE, PHI, OMIS-I, OMIS-II, etc.) were developed by various enterprises and research organizations. However, it was not until 2000 that the first hyperspectral imaging spectrometer Hyperion was sent into space aboard the EO-1 satellite. Covering the contiguous wavelength range from 0.4 to 2.5 μm in 242 overlapping bands, this instrument had worked until 2017 and provided about 90 000 images by user requests and in response to unusual or extreme events [9].

Between 2000 and 2020, 25 hyperspectral imagers were deployed in space [10]. In addition to well-known diffraction gratings and sensor arrays with push broom scanning, these instruments use several other spectral separation techniques, such as linear variable filters [11], acousto-optic tunable filters [12], or tunable Fabry–Pérot filters [13]. At least one hyperspectral imager is known to combine interferometry and a Fourier transform algorithm for the restoration of spectra [14]. The above designs differ not only in the resultant spectral resolution but also in production costs.

Today, when more than two decades of the new century have passed, some general trends concerning multispectral and hyperspectral remote sensing can be traced. Having turned from unique devices designed for a specific mission into commercially available instruments, hyperspectral cameras still remain quite expensive. High prices impede a wider application of multispectral and hyperspectral data, especially in developing countries, where they could be particularly useful [15–17]. At the same time, installing a compact sensor on an unmanned aerial vehicle (UAV) instead of a conventional manned aircraft can greatly reduce the survey cost [18].

The perception of multispectral imaging has changed as well, both from technological and marketing point of view. A number of consumer-grade UAVs are marketed as intended for multispectral surveys while either carrying a conventional RGB camera and a near infrared (NIR) one, or just a single NIR sensitive camera with an optical filter to switch between the visible and the NIR range [16]. On the other hand, newly proposed techniques for environmental monitoring conform to these limitations; thus, a number of vegetation indices rely on the observed brightness of an object in wide spectral bands (red, green, blue, and NIR) [19] rather than linking "one spectral band" to "one biogeophysical variable" [7].

The commercial availability of affordable CCD and complementary metal–oxide semiconductor (CMOS) sensors has boosted the development of low-cost multispectral cameras, including by educators and enthusiasts [17, 20–27]. Some of their designs return to the idea of separating spectral bands with optical filters, using either a separate sensor for each band or a single sensor with a set of interchangeable filters. In the laboratory environment, some researchers experiment with illuminating the object of study with narrow-band light, mainly from light-emitting diodes [25]. Such low-cost devices provide adequate results at moderate cost, and their data are used to solve a variety of problems, from monitoring vegetation [19, 22–23] to identifying fish species [24] and assessing the quality of fruit [26, 27].

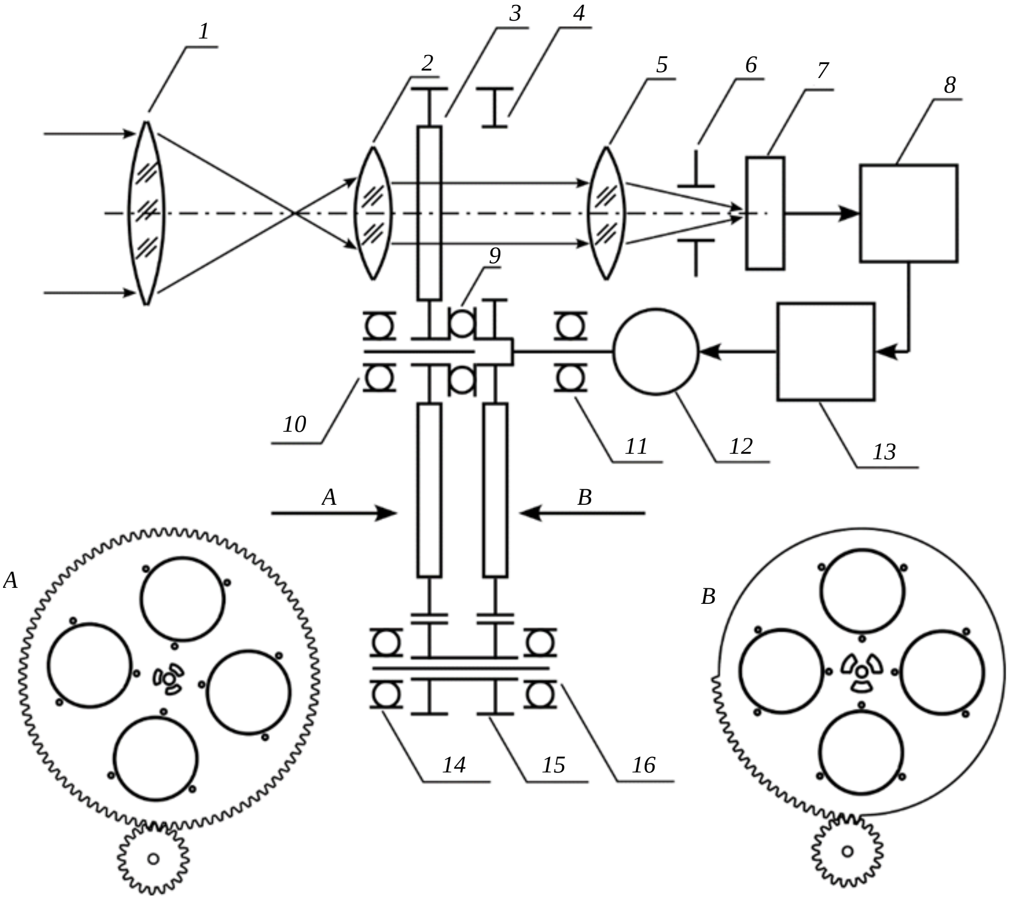

Рис. 1. Общая оптико-механическая схема многоспектральной камеры

Fig. 1. Optical and mechanical design of the multispectral camera

In this paper, we present a new portable multispectral camera for environmental monitoring in the field. Its optical, mechanical, and electronic design is described, along with some results of vegetation observations and vegetation indices distributions calculated from the data obtained.

Materials and methods. A general scheme of the developed multispectral camera is presented in Fig. 1. The device comprises a single CMOS sensor *7*, with a set of interchangeable interference filters installed in two wheels *3* and *4* for spectral selection. A Raspberry Pi 4 single-board computer *8* controls both the mechanical part and the processes of image acquisition and storage. A detailed description of the design is presented in the following sections.

Sensor. Low-cost CMOS image sensors are frequently used when designing cameras for experimental and educational purposes. Several companies have designed and marketed their own brands of sensors, such as IMX219 [17] and IMX036 [20] by Sony, VCXU-13M by Baumer [21], OV7670 [23] and OV5647 [25] by OmniVision.

When developing the device, OV5647 by OmniVision was used as the basis. This is a 5-megapixel CMOS sensor intended for use in a wide range of low-cost applications, from toys to cellular phone cameras. The sensor is capable of operating with a frame rate of up to 15 fps in 2592 × 1944 pixels maximum resolution. The image quality, data rate, and other sensor parameters can be controlled through a proprietary Serial Camera Control Bus (SCCB), easily compatible with Raspberry Pi single-board computers. The automatic image control functions of the sensor include exposure control, white balance and black level calibration, as well as band filtering and 50/60 Hz luminance detection [28].

A conventional red–green–blue (RGB) image is obtained by applying a mask of wideband bandpass filters to the sensor surface. The filters are arranged in a Bayer pattern, half of them being green, one quarter being blue, and one quarter being red, to mimic the sensitivity distribution of the human eye. Fig. 2 shows the resulting spectral distribution of the sensor quantum efficiency [25].

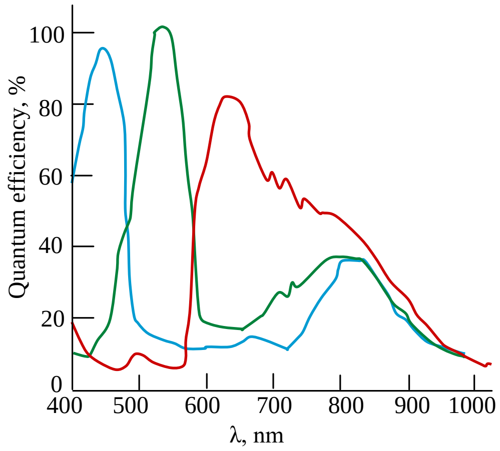

Рис. 2. Спектральное распределение квантовой эффективности фотоприемной матрицы OV5647

Fig. 2. Spectral distribution of the quantum efficiency of the OV5647 image sensor

Higher values correspond to a higher output from the same number of incoming photons. It can be noticed that the curves overlap; therefore, radiation with a wavelength of about 500 nm would affect both the blue and the green channel, while 600 nm affects the green and the red channel. In addition, the efficiency of the red channel increases slightly at the ultraviolet edge of the working range.

Since the sensor array is silicon-based, all three channels show some sensitivity in the near infrared (NIR) spectral region, between 700 and 1000 nm, where the color filters are transparent. In order to exclude the infrared radiation and obtain images exclusively in the visible part of the spectrum, a filter coating may be applied by the manufacturer, either to the sensor array itself or to the objective lens. To cover the widest possible range of sensitivity, we used a sensor without an infrared filter coating, labeled as "NoIR" by the manufacturer.

Spectral selectivity. In order to isolate a narrow spectral region of interest, the camera was equipped with switchable interference filters. Their number is naturally limited by the optical and mechanical design of the camera; therefore, those spectral bands that describe the nature and condition of an object with maximum accuracy should be selected.

The intensity of light coming from an object to the camera is defined by the product of the object's reflection coefficient and intensity of incident light from the source that irradiates the object. Since the Sun is known to be a thermal radiation source with a continuous spectrum in the visible and near infrared regions, selection of spectral channels may focus on the spectral features of the object of study.

For plants, these features are formed by pigments contained in the cells, which play an important role in the plant biochemistry. Tab. 1 lists a number of spectral features linked to absorption by chlorophylls, carotenes, and xanthophylls.

As far as monitoring of animals is concerned, the number of available scientific publications is limited. Some examples include assessment of

Табл. 1. Спектральные признаки растительных пигментов

Tab. 1. Spectral features of plant pigments

λ, nm	Feature description	References
435	Chlorophyll *a* absorption maximum	[29]
485	β carotene absorption minimum, and an intersection between its spectrum and the chlorophyll *b* spectrum	[29]
500	An intersection between chlorophyll *a* and *b* absorption minima, and an absorption maximum of β carotene	[29]
510	Carotenoids absorption maximum	[30]
550	An intersection between chlorophyll *a* and *b* absorption minima	[29]
620	An intersection between chlorophyll *a* and *b* absorption minima	[29]
670	Chlorophyll *a* absorption maximum	[29]
677	A spectral feature for differential observation of the xanthophyll cycle	[30]
700	The "red edge" of absorption by chlorophyll and carotenoids	[31]
735	Chlorophyll *a* and *b* absorption minima	[29]
750	Reference wavelength for chlorophyll content assessment	[32]
803	A spectral feature for differential observation of the xanthophyll cycle	[30]

Табл. 2. Параметры интерференционных фильтров

Tab. 2. Parameters of interference filters

Central wavelength, nm	τ_{max}	FWHM, nm
430	0.49	12
500	0.19	17
530	0.18	19
580	0.23	12
620	0.26	13
761	0.16	13

populations of wild birds [33, 34], identification of beef cattle [35, 36], wild elks, horses [36], and mule deer [37]. Large-sized individual animals, such as wildebeests, zebras [38], and polar bears [39], are detectable in imagery of very high resolution obtained from commercial satellites. Marine mammals, e. g., southern right whales [40] and Weddell seals [41] have also been the object for multispectral imaging. In their case, the task of remotely detecting an underwater animal becomes more difficult, necessitating consideration of optical properties of water to provide the required contrast between the animal and the background.

Given the above considerations and the range of available models, six filters were selected, with their parameters given in Tab. 2. Maximal transmission τ_{max} and full width at half maximum (FWHM) were measured using a compact fiber spectrometer.

Optical design. Unlike wideband optical filters, interference filters operate by reflecting, rather than absorbing, unnecessary light. In a thin dielectric layer, light with wavelength λ will be reflected in case the optical path difference between its parts reflected from the two surfaces of the layer equals an integer multiple of the light wavelengths:

$$2n_2 d\cos(\theta_2) = m\lambda, \quad (1)$$

where n_2 is the refraction index of the layer with respect to the medium from where the light is coming, d is its thickness, θ_2 is the angle of incidence on the rear surface of the layer, and $m \in \mathbb{Z}$. At the same time, θ_2 depends on the angle of incidence on the front surface of the layer. Therefore, the wavelength of maximum transmission depends on the filter orientation with respect to the light beam.

In a conventional converging lens, the field of view is limited by the angle between the two chief rays that pass through the center of the lens to the opposite edges of the sensor. None of the chief rays are ever parallel to the lens optical axis, either before or after the lens, except for the only ray that passes along the axis. Therefore, for any position of an interference filter, the wider the field of view, the greater the spectral shift between the center of the image and its edges. Conversely, a perfectly parallel light beam would reach the filter at a constant angle, and the transmission function would be the same for any point in the image.

A parallel beam was formed using two successive confocal lenses (*1* and *2* in Fig. 1): the rear focal plane of the first lens coincides with the front focal plane of the second lens. After passing through a filter in one of wheels – *3* or *4*, the light beam is converged once again by lens *5*. Image sensor *7* is installed on a moveable mount; since no corrections were applied for chromatic aberrations, to adjust the image sharpness, the sensor has to be shifted along the camera axis by manually rotating a leadscrew.

A factory-made iris diaphragm *6* is installed between the final lens and the sensor. By limiting the maximal angle of incidence for light reaching the sensor, it reduces aberrations and increase the depth of field.

Fig. 3 details the optical design of the developed camera and shows the distances between the elements with their respective diameters. L1 to L3 are the lenses, F denotes the interference filter, A is the aperture diaphragm, and S is the front surface of the sensor. All the dimensions are given in millimeters. Distances to focal points were measured in natural daylight, taken from the corresponding glass surfaces rather than from the principal planes of the lenses (see the diagram).

All the mounts that support lenses and other optical elements were printed using a fused deposition modeling (FDM) technique. The mounts are

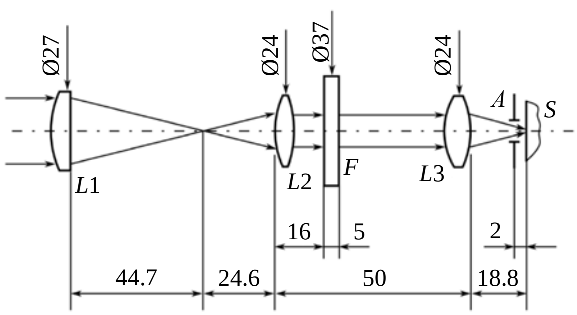

Рис. 3. Оптическая схема многоспектральной камеры

Fig. 3. Optical design of the multispectral camera

installed along an aluminum alloy beam, facilitating their positioning during the necessary adjustments. To protect the sensor from stray light, the optical system is enclosed in two cylindrical plastic casings (before and after the filter block), produced also using 3D printing; the inner surfaces of the casings are painted matte black.

Mechanical design. Due to the considerable dimensions of available filters (46 mm in diameter together with the frame), installing more than four of them in a single wheel would make that wheel inconveniently large. Therefore, two parallel wheels (*3* and *4*, Fig. 1) were designed to carry three filters each, with one circular opening left empty. To compensate for the resulting displacement of the wheel's center of mass, gauged weights were glued to its surface. Since two consequent filters would obviously block out all the incoming light, at least one of the empty openings always stays in the optical path when the wheels are stopped.

The filter wheels rotate in a manner that resembles a mechanical counter. The rear wheel *4* is rotated directly by a Nema 17 stepper motor *12*, which is controlled by the Raspberry Pi computer *8* through an A4988 driver *13*. The front wheel *3* is driven through an additional geared wheel *15*. However, since only a quarter of the rear wheel's rim has teeth (see insets *A* and *B* in Fig. 1), a full revolution of the rear wheel corresponds to the front wheel being rotated by 90°, thus switching to the neighboring filter.

All three geared wheels rotate on steel axles that have their ends set in ball bearings *10*, *11*, *14*, and *16*. To ensure the necessary spacing between the filter wheels while keeping them parallel, a thrust ball bearing *9* is placed between them. The entire mechanical setup is held upright by two flat mounts.

Various techniques were used to create the mechanical parts of the camera. Geared wheels were printed out of polylactide (PLA) and polyethylene terephthalate (PET-G) using the FDM technique. The ball bearings *10*, *11*, *14*, and *16* were factory made, and the thrust bearing *9* consists of two cups printed out of PLA, with steel balls placed between them. The mounts were cut out of acrylic glass using laser cutting.

Software, data acquisition and processing. Controlling the camera, image acquisition and storage are performed by a Raspberry Pi 4 Model B running Raspberry Pi OS, which is a fork of Debian Linux, intended for use with single-board computers.

A script in Python was written for image acquisition, working in the following manner. First, using the Picamera2 library, sensor settings are updated, including setting the exposure time, the analogue gain ratio, and disabling the automatic white balance. Then, while showing a preview in a separate window, a frame is captured and stored as an array of raw values. Considering the output resolution of the sensor, this array contains 3 × 2592 × 1944 integer numbers ranging from 0 to 255. It is then split into three separate arrays of 2592 × 1944 elements each, and four quartiles (at 0, 0.25, 0.75, and 1.0) are calculated and displayed for each of these arrays. Provided that the brightness distribution in the channel of interest is suitable, the entire raw array is written to a file with a name representing the object of study, the filming date, and the spectral band. Otherwise, the exposure time is adjusted, and a new frame is captured, starting the loop over.

Processing and analysis of acquired images is carried out by a separate PC, following a routine similar to the one described above, splitting the raw arrays, generating preview images, and performing element-wise operations on arrays. Among the software packages used are NumPy, Pillow, and Matplotlib libraries.

Results. Fig. 4 presents the general appearance of the developed multispectral camera. External connections, such as 5 volts USB power, the keyboard, the mouse, and the monitor, are not shown in the photo.

After completing the assembly and the corresponding adjustments, several tests were performed to assess the resulting size of the field of view and its spectral homogeneity, as well as to check the feasibility of obtaining distributions of vegetation indices.

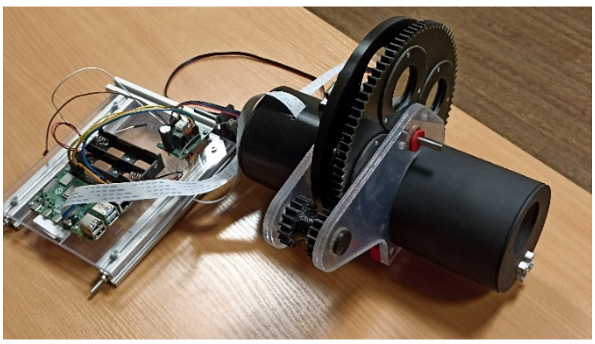

Рис. 4. Внешний вид многоспектральной камеры
Fig. 4. General appearance of the multispectral camera

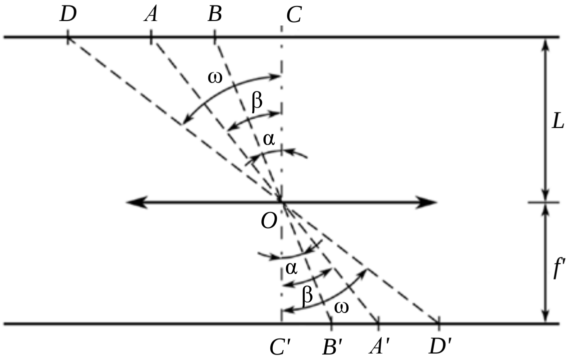

Рис. 5. Геометрические соотношения между фокусным расстоянием и размером поля зрения

Fig. 5. Geometrical interrelations between the focal length and the field of view size

Field of view assessment. The field of view and focal length of the camera were measured relying on the geometrical optics approximation. In Fig. 5, *AB* is an object placed at a distance *L* from the optical system of the camera (presented as a single converging lens for simplicity), and *A*'*B*' is its image in the focal plane. *CC*' is the optical axis of the lens, and $L >> 2f'$ is large enough not to affect the transverse magnification of the system.

Light rays passing through the lens center *O* do not change their direction. Therefore, three pairs of similar triangles are formed, in which $\angle BOC = \angle B'O'C' = \alpha$, $\angle AOC = \angle A'O'C' = \beta$, $\angle DOC = \angle D'O'C' = \omega$ (which equals half the angular size of the field of view of the camera). Then,

$$\tan\alpha = \frac{BC}{L} = \frac{B'C'}{f'};$$
$$\tan\beta = \frac{AC}{L} = \frac{A'C'}{f'}; \qquad (2)$$
$$\tan\beta - \tan\alpha = \frac{AB}{L} = \frac{A'B'}{f'},$$

where f' is the lens rear focal length. From (2), we can calculate this distance by taking a picture of an object with known dimensions, measuring the distance to this object, and then using the pixel size from the sensor datasheet P_x to convert the object image size *X* from pixels to meters:

$$f' = L\frac{XP_x}{AB}. \qquad (3)$$

Then, considering the triangle $\triangle C'OD'$, we calculate the angular size of the field of view:

Табл. 3. Сравнение параметров четырех оптических систем

Tab. 3. Comparison of parameters of four optical designs

Optical system	*AB*, mm	*L*, m	*f* ', mm	2ω, …°
Multispectral camera	297	32.5	58.2	3.6
Wide-angle	479	4.1	2.0	83.6
Normal	479	4.1	3.3	57.1
RSS	9	4.0	148.8	1.4

$$2\omega = 2\operatorname{atan}\left(\frac{bP_x}{2f'}\right), \qquad (4)$$

where *b* = 2592 is the corresponding sensor size in pixels.

Measurements and calculations using (3) and (4) were performed for the designed optical system, as well as for three other camera lenses: a wide-angle lens and a normal one, both shipped with CMOS cameras, and a telephoto lens from the RSS portable spectrometer [3]. The resulting values are presented in Tab. 3.

Spectral homogeneity assessment. This test was aimed at assessing the angular uniformity of the camera spectral transmission and sensitivity, i. e., at assessing the difference in the sensor response to spectrally identical radiation over the image plane.

Assuming the daylight from the overcast sky to be sufficiently parallel and uniform over the field of view of the camera, we took a number of pictures directing the camera toward the same point in the sky and using the same 580 nm interference filter for each of the lenses. It can be seen from Fig. 2 that, at this wavelength, both the red and the green channel show considerable sensitivity. In an ideal case, with light passing through the filter in a completely parallel beam and the CMOS sensitivity being the same for each of its elements, the pictures would be uniformly filled with a single color, corresponding to a constant ratio of red and green channels values. Actual ratio distributions obtained in the experiment are presented in Fig. 6.

For clarity, horizontal cross-sections are presented in Fig. 7, going through the centers of the two-dimensional distributions shown in Fig. 6.

Vegetation index test. A wide multitude of spectral indices has been proposed to discern between different plant species and remotely assess their health and ecological condition [19]. In this

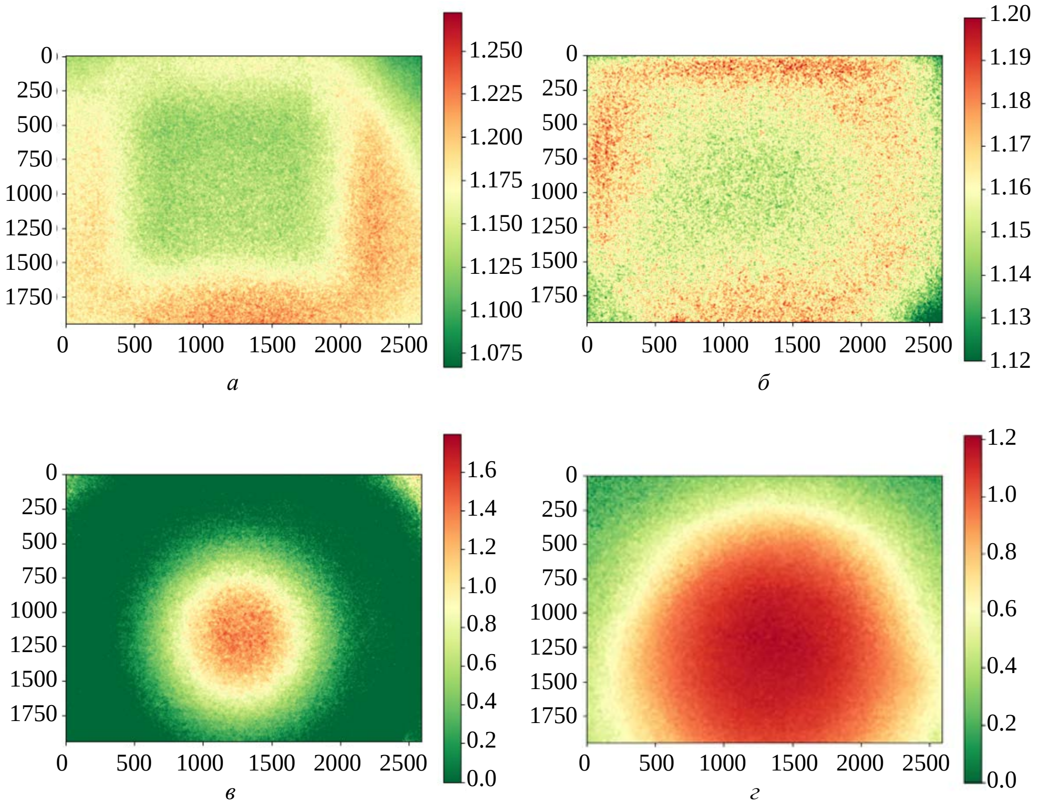

Рис. 6. Двумерные распределения отношения выходных сигналов в красном и зеленом каналах R/G: *а* – многоспектральная камера; *б* – телеобъектив РСС; *в* – широкоугольный объектив; *г* – нормальный объектив

Fig. 6. Two-dimensional distributions of the ratio of responses in the red and the green channels R/G: *а* – multispectral camera; *б* – RSS telephoto lens; *в* – wide-angle lens; *г* – normal lens

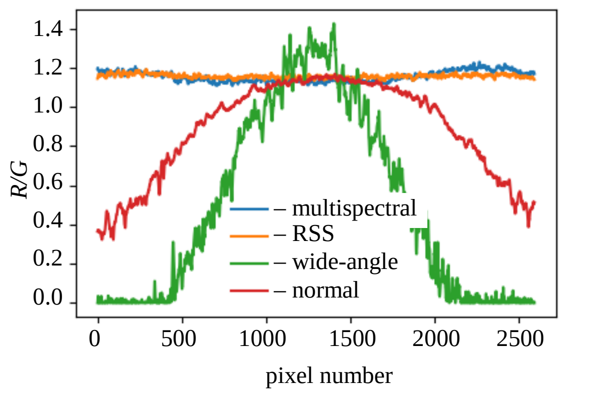

Рис. 7. Распределения отношений значений R/G вдоль горизонтальной линии через центр кадра

Fig. 7. R/G ratio distributions along a horizontal line through the center of the frame

experiment, we attempted to obtain spatial distributions of two vegetation indices, GRVI and NDVI, using narrow spectral bands corresponding to the features in a typical vegetation spectrum.

Images of trees and shrubs were taken from a distance of 40…60 m, in clear sunny weather, mostly in the afternoon hours. Before calculating the distributions, all the values in the corresponding arrays were normalized, i. e., transformed from the 0…255 range to the 0–1 range:

$$X_{\text{norm}} = \frac{X - X_{\min}}{X_{\max} - X_{\min}},$$

where $X_{\max}$, $X_{\min}$ are the maximal and minimal values in the array X (either red, green, or blue).

The red–green vegetation index, as its name suggests, relies on the difference in brightness between the green spectral region (reflection maximum of green plants) and the red spectral region (corresponding reflection minimum) [42]. Its values lie between –1 and +1: high positive values correspond to vegetation, soils and rocks are characterized by values close to zero, and negative values correspond to various non-plant objects.

Considering the wavelengths in Tab. 1, we used the response values of the green channel from a frame taken in the 530 nm spectral band (G_{530}) and those of the red channel obtained in the

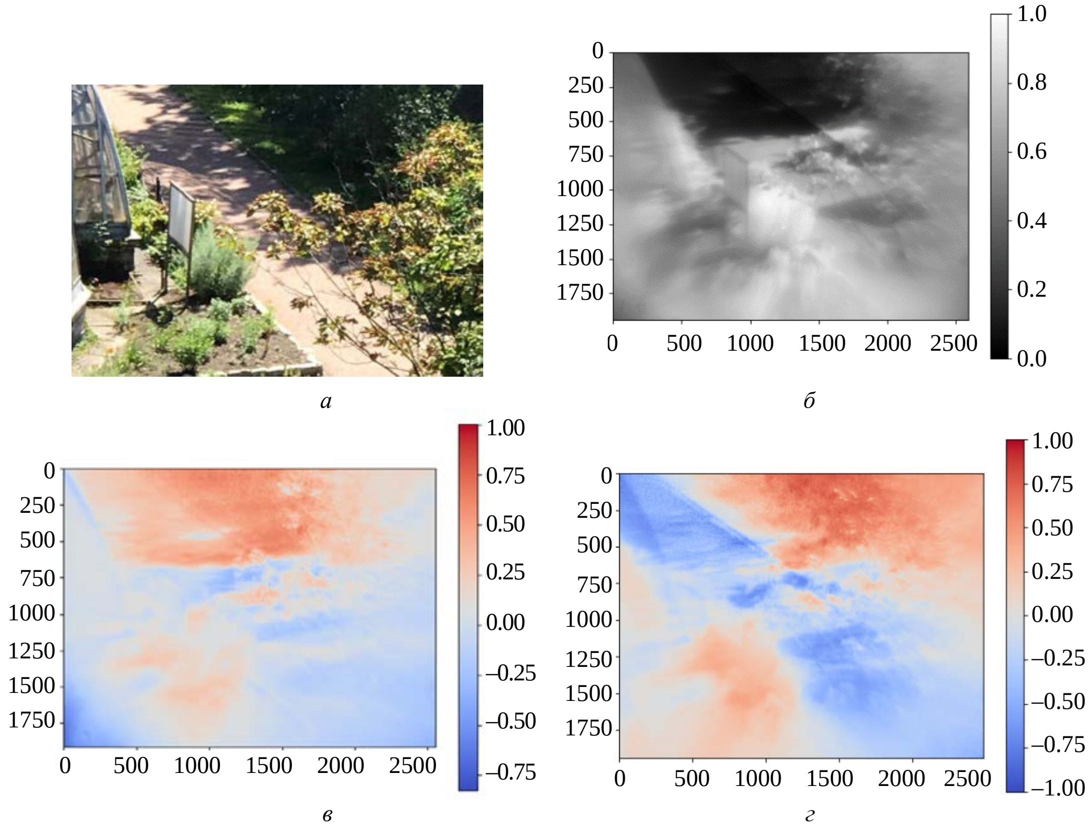

Рис. 8. Результаты многоспектральной съемки участка аллеи, окруженного деревьями: *а* – фото участка камерой мобильного телефона; *б* – снимок многоспектральной камерой в отсутствие фильтров; *в* – распределение индекса GRVI; *г* – распределение индекса NDVI

Fig. 8. Results of a multispectral survey of an alley part surrounded by trees: *а* – photo of the area taken with a smartphone camera; *б* – an image taken by the multispectral camera with no filter used; *в* – GRVI distribution; *г* – NDVI distribution

620 nm band (R_{620}):

$$\mathrm{GRVI} = \frac{G_{530} - R_{620}}{G_{530} + R_{620}}.$$

The normalized difference vegetation index (NDVI) was proposed as early as 1970s for remote assessment of crop health [19]. It is based on comparison between values in the red reflection minimum and in the near infrared region, in which reflection of green leaves begins to rise steeply. Similar to the previous index, its values lie within the region between –1 and +1, with similar patterns.

This index was calculated using red channel values from the 620 and 761 nm bands (R_{620} and R_{761} correspondingly):

$$\mathrm{NDVI} = \frac{R_{761} - R_{620}}{R_{761} + R_{620}}.$$

As an example of the results obtained, Fig. 8 demonstrates a gravel alley in a park, with green trees surrounding and branches overhanging. Fig. 9 depicts a coniferous tree (hybrid larch, *Larix czekanowskii* Szafer) and two deciduous trees in the background (a silver poplar, *Populus alba* L., and a common alder, *Alnus glutinosa* (L.) Gaertn.). In both figures, a conventional RGB photo of the site is given first, which may not accurately reflect the multispectral images due to the differences between the optical designs of the cameras used.

Discussion. In this study, we have designed and successfully tested a portable multispectral camera for ecological monitoring of vegetation cover. From the standpoint of the camera focal length and its field of view (Tab. 3), the selected optical design is a telephoto lens similar to that of the RSS spectrometer. At the same time, the two designs provide comparable spectral homogeneity of the frame, even though the field of view of the camera is twice as large. Considering the curves in Fig. 7, the mean ratio of channel values for the RSS lens is $\overline{R/G} = 1.16$, and the standard devia-

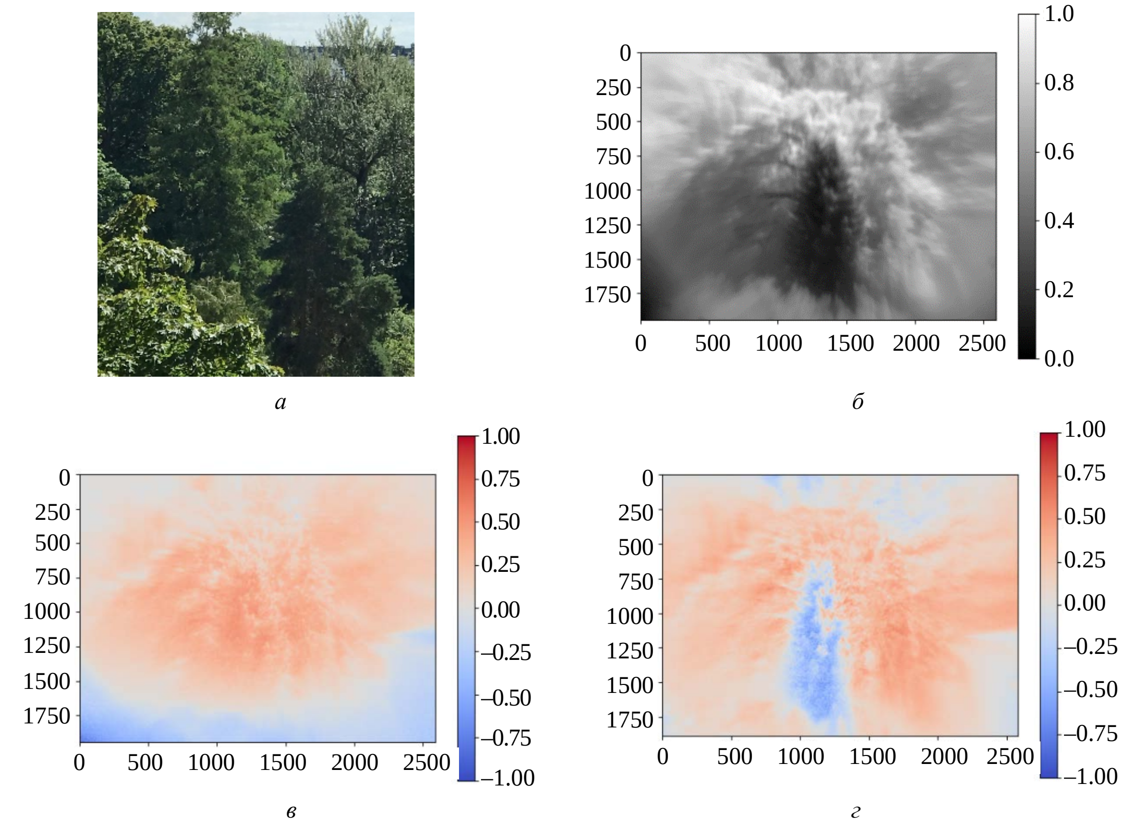

Рис. 9. Результаты многоспектральной съемки участка парка с хвойным и лиственными деревьями: *а* – фото участка камерой мобильного телефона; *б* – снимок многоспектральной камерой в отсутствие фильтров; *в* – распределение индекса GRVI; *г* – распределение индекса NDVI

Fig. 9. Results of a multispectral survey of a park area with a coniferous tree and deciduous trees: *а* – photo of the area taken with a smartphone camera; *б* – an image taken by the multispectral camera with no filter used; *в* – GRVI distribution; *г* – NDVI distribution

tion is $\sigma = 0.011$, while for our lens design, $\overline{R/G} = 1.16$ and $\sigma = 0.027$.

No preliminary numeric simulation of the optical design was performed. In future research, a thorough selection of elements will refine the design and reduce chromatic aberrations, decreasing the necessary sensor movement and improving the quality of the images produced.

The results obtained leave the choice of OV5647 as the image sensor open to question. The Bayer filters allow for some additional capabilities, such as the aforementioned experiment on spectral homogeneity, while also possibly rejecting wavelengths that correspond to $m > 1$ in (1) (higher orders of interference). In our case, however, the interference filters are based on colored glass for rejection of higher orders. Moreover, when taking an image through an interference filter, only one of the RGB channels would work, with the other two producing no more than dark rectangles. This means that only a third of the raw file would contain meaningful data. Overall, a monochrome sensor in the same design but without Bayer filters would likely perform better.

In addition, we performed no demosaicing during data processing to determine the exact correspondence between values in the raw data and exposure for each of the physical pixels. We will address will this task in future research.

The camera design was created bearing the idea of a low-cost approach. The interference filters form the costliest part of the device; market prices of similar parts range from 15 to 200 US dollars, depending on the maximum value and width of the transmission band. Another major spending was the Raspberry Pi single-board computer (about 150 US dollars). The costs of 3D printing are harder to assess; however, the printed parts make the basis of the mechanical design. Laser cutting of acrylic glass, on the other hand, can be replaced by manual treatment.

In scientific publications, the costs associated with the design of devices are frequently omitted, even when declaring the aim of developing low-cost constructions. In cases when the expenditures are mentioned, the cost may range from about 100 euros (comprising two cameras and a multiplexer chip) [17] to below 2000 euros for a more sophisticated system [23]. The design that we propose falls into the lower part of this range.

Concerning commercially available multispectral cameras, their prices are generally incomparably higher. For example, the DJI P4 Multispectral UAV [16] is marketed at about 10 thousand US dollars. When comparing this price to similar UAVs by DJI but capable of RGB imaging only, one can presume that the P4 Multispectral six-channel camera accounts for nearly half of the sum. Morales et al. state a price of about 5000 euros for a RedEdge-MX multispectral camera, "one of the golden references" on the market [23].

The conducted vegetation survey has confirmed the suitability of the developed camera for obtaining distributions of GRVI and NDVI indices. Both indices performed well in the task of separating vegetation from non-plant objects (Fig. 8, *в*, *г*). However, GRVI turned out to be more susceptible to errors emerging from differences in solar irradiation and the depth-of-field effect. In Fig. 8, *в*, the farthest, shadowed part of the alley shows high positive values falsely, while, in Fig 9, *в*, low negative values appear along the lower border of the frame where the plants were nearest to the camera. On the other hand, NDVI was negative for the coniferous tree (Fig. 9, *г*), which had a much lower reflectivity in the NIR than the background foliage, and therefore appeared darker in Fig. 9, *б*.

The current camera design includes a set of filters that features wavelengths through the entire visible range into near infrared. This can be redundant for determination of a certain vegetation index. However, with this comprehensiveness and the relative ease of replacing filters in their wheel sockets, the portable multispectral camera can be useful for determining the best-suited spectral bands when addressing a new problem in remote monitoring of vegetation. Based on the data obtained through its use, simpler and easier to manufacture designs can be proposed for specific tasks.

Авторский вклад

Горяинов Виктор Сергеевич – разработка оптической схемы многоспектральной камеры; написание текста статьи.

Нгуа Ндонг Авеле Жак Бернис – проведение лабораторных испытаний многоспектральной камеры; обработка и анализ полученных данных.

Мазоя Адам Бенджамин – разработка механической схемы многоспектральной камеры; участие в лабораторных испытаниях.

Тарасов Сергей Анатольевич – общее руководство проектом; редактирование текста статьи.

Author`s contribution

Viktor S. Goryainov, creation of the optical design of the multispectral camera; writing the article text.

Jacques B. Ngoua Ndong Avele, performing laboratory tests of the multispectral camera; processing and analyzing the data obtained.

Adam B. Mazoya, creation of the mechanical design of the multispectral camera; participation in the laboratory tests.

Sergey A. Tarasov, general supervision of the project; editing the article's text.

Список литературы

1. Krinov E. L. Spectral reflectance properties of natural formations. Ottawa: National research council of Canada, 1953. 268 p.

2. Buznikov A. A. Space spectrophotometry of the natural environment from manned orbital stations // J. of Optical Technology. 2015. Vol. 82, № 7. P. 487–493. doi: 10.1364/JOT.82.000487

3. Горяинов В. С., Бузников А. А., Костиков Е. В. Модернизация портативного спектрометра РСС // Изв. СПбГЭТУ "ЛЭТИ". 2020. № 2. С. 5–16.

4. Raizer V. Optical remote sensing of ocean hydrodynamics. Boca Raton: CRC Press, 2019. 296 p. doi: 10.1201/9781351119184

5. Barnett T. L., Juday R. D. Skylab S191 visible-infrared spectrometer // Applied Optics. 1977. Vol. 16, № 4. P. 967–972. doi: 10.1364/AO.16.000967

6. Goetz A. F. H., Srivastava V. Mineralogical mapping in the Cuprite Mining District, Nevada // Proc. of the Airborne Imaging Spectrometer Data Anal. Workshop. Pasadena. Jet Propulsion Laboratory, 1985. P. 22−31.

7. Goetz A. F. H. Three decades of hyperspectral remote sensing of the Earth: a personal view // Remote Sensing of Environment. 2009. Vol. 113. P. S.5–S.16. doi: 10.1016/j.rse.2007.12.014

8. Vane G., Goetz A. F. H., Wellman J. B. Airborne Imaging Spectrometer: a new tool for remote sensing // IEEE Trans. Geosci. Remote Sens. 1984. Vol. GE-22, № 6. P. 546–549. doi: 10.1109/TGRS.1984.6499168

9. Hyperion: the first global orbital spectrometer, Earth Observing-1 (EO-1) satellite (2000–2017) / E. M. Middleton, P. K. E. Campbell, L. Ong, D. R. Landis, Q. Zhang, C. S. Neigh, K. F. Huemmrich, S. G. Ungar, D. J. Mandl, S. W. Frye, V. T. Ly, P. G. Cappelaere, S. A. Chien, S. Franks, N. H. Pollack // IEEE Intern. Geoscience and Remote Sensing Symp. (IGARSS), Fort Worth, 23–28 July 2017. IEEE, 2017. P. 3039–3042. doi: 10.1109/IGARSS.2017.8127639

10. Qian S.-E. Hyperspectral satellites, evolution, and development history // IEEE J. of Selected Topics in Applied Earth Observations and Remote Sensing. 2021. Vol. 14. P. 7032–7056. doi: 10.1109/JSTARS.2021.3090256

11. HyperScout-1 inflight calibration and product validation / I. Benhadj, S. Livens, M. Esposito, N. Vercruyssen, C. Van Dijk, M. Soukup, A. Z. Marchi, L. Maresi // Intern. J. of Remote Sensing. 2024. Vol. 45, № 7. P. 2486–2517. doi: 10.1080/01431161.2024.2331979

12. Visible and near-infrared imaging spectrometer aboard Chinese Chang'E 3 spacecraft / J. Wang, Z. He, R. Shu, R. Xu, K. Chen, C. Li // Optical Payloads for Space Missions. Chichester: Wiley, 2016. P. 121–139. doi: 10.1002/9781118945179.ch5

13. Miniature spectral imager in-orbit demonstration results from Aalto-1 nanosatellite mission / J. Praks, P. Niemelä, A. Näsilä, A. Kestilä, N. Jovanovic, B. Riwanto, T. Tikka, H. Leppinen, R. Vainio, P. Janhunen // IEEE Intern. Geoscience and Remote Sensing Symp., Valencia, 22–27 July 2018. IEEE, 2018. P. 1986–1989. doi: 10.1109/IGARSS.2018.8517658

14. Overview of the Fourier Transform Hyperspectral Imager (HSI) boarded on HJ-1A satellite / X. Zhao, Z. Xiao, Q. Kang, Q. Li, L. Fang // IEEE Intern. Geoscience and Remote Sensing Symp., Honolulu, 25–30 July 2010. IEEE, 2010. P. 4272–4274. doi: 10.1109/IGARSS.2010.5649250

15. Artisanal exploitation of mineral resources: remote sensing observations of environmental consequences, social and ethical aspects / N. M. Ngom, D. Baratoux, M. Bolay, A. Dessertine, A. A. Saley, L. Baratoux, M. Mbaye, G. Faye, A. K. Yao, K. J. Kouamé // Surveys in Geophysics. 2023. Vol. 44. P. 225–247. doi: 10.1007/s10712-022-09740-1

16. High-resolution multispectral and RGB dataset from UAV surveys of ten cocoa agroforestry typologies in Côte d'Ivoire / S.-K. Lammoglia, Y. L. Akpa, J. H. Danumah, Y. L. A. Brou, J. N. Kassi // Data in Brief. 2024. Vol. 55. Art. № 110664. doi: 10.1016/j.dib.2024.110664

17. Raspberry Pi 3 multispectral low-cost sensor for UAV based remote sensing. Case study in south-west Niger / E. Belcore, M. Piras, A. Pezzoli, G. Massazza, M. Rosso // ISPRS. 2019. Vol. XLII-2/W13. P. 207–214. doi: 10.5194/isprs-archives-XLII-2-W13-207-2019

18. Hyperspectral imaging: a review on UAV-based sensors, data processing and applications for agriculture and forestry / T. Adão, J. Hruška, L. Pádua, J. Bessa, E. Peres, R. Morais, J. J. Sousa // Remote Sens. 2017. Vol. 9, № 11. Art. № 1110. doi: 10.3390/rs9111110

19. Review: cost-effective unmanned aerial vehicle (UAV) platform for field plant breeding application / G. Jang, J. Kim, J.-K. Yu, H.-J. Kim, Y.-H. Kim, D.-W. Kim, K.-H. Kim, C. Lee, Y. S. Chung // Remote Sensing. 2020. Vol. 12, № 6. Art. № 998. doi: 10.3390/rs12060998

20. Баранов П. С., Чиркунова А. А. Телевизионная камера видимого и ближнего инфракрасного диапазонов // Изв. вузов России. Радиоэлектроника. 2015. Вып. 4. С. 47–56.

21. Овчинников А. В. Многоспектральная камера с последовательным формированием изображений // Журн. радиоэлектроники. 2021. № 5. С. 1–11. doi: 10.30898/1684-1719.2021.5.6

22. Mazeh F., El Sahili J., Zaraket H. Low-cost NDVI platform for land operation: passive and active // IEEE Sensors Let. 2021. Vol. 5, № 10. Art. № 5500804. doi: 10.1109/LSENS.2021.3112822

23. A multispectral camera development: from the prototype assembly until its use in a UAV system / A. Morales, R. Guerra, P. Horstrand, M. Diaz, A. Jimenez, J. Melian, S. Lopez, J. F. Lopez // Sensors. 2020. Vol. 20. Art. № 6129. doi: 10.3390/s20216129

24. Classification of fish species using multispectral data from a low-cost camera and machine learning / F. Monteiro, V. Bexiga, P. Chaves, J. Godinho, D. Henriques, P. Melo-Pinto, T. Nunes, F. Piedade, N. Pimenta, L. Sustelo, A. M. Fernandes // Remote Sensing. 2023. Vol. 15. Art. № 3952. doi: 10.3390/rs15163952

25. Portable multispectral imaging system based on Raspberry Pi / N. Lopez-Ruiz, F. Granados-Ortega, M. A. Carvajal, A. Martinez-Olmos // Sensor Review. 2017. Vol. 37, № 3. P. 322–329. doi: 10.1108/SR-12-2016-0276

26. Noguera M., Millan B., Andújar J. M. New, low-cost, hand-held multispectral device for in-field fruit-ripening assessment // Agriculture. 2023. Vol. 13, № 1. P. 4. doi: 10.3390/agriculture13010004

27. Wavelength selection of multispectral imaging for oil palm fresh fruit ripeness classification / M. Shiddiq, H. Herman, D. S. Arief, E. Fitra, I. R. Husein, S. A. Ningsih // Applied Optics. 2022. Vol. 61, № 17. P. 5289–5298. doi: 10.1364/AO.450384

28. OmniVision. OV5647 datasheet. Preliminary specification. URL: https://cdn.sparkfun.com/datasheets/

Dev/RaspberryPi/ov5647_full.pdf (дата обращения: 09.06.2025).

29. Goryainov V. S., Buznikov A. A. A study of the influence of copper sulfate on the spectral properties of common buckwheat (Fagopyrum esculentum) // J. of Physics: Conf. Ser. 2021. Vol. 2103, № 1. Art. № 012155.
doi: 10.1088/1742-6596/2103/1/012155

30. Sonobe R., Wang Q. Assessing the xanthophyll cycle in natural beech leaves with hyperspectral reflectance // Functional Plant Biology. 2016. Vol. 43, № 5. P. 438–447.
doi: 10.1071/FP15325

31. Assessing Carotenoid Content in Plant Leaves with Reflectance Spectroscopy / A. A. Gitelson, Y. Zur, O. B. Chivkunova, M. N. Merzlyak // Photochem. Photobiol. 2002. Vol. 75, № 3. P. 272–281.
doi: 10.1562/0031-8655(2002)0750272ACCIPL2.0.CO2

32. Sims D. A., Gamon J. A. Relationships between leaf pigment content and spectral reflectance across a wide range of species, leaf structures and developmental stages // Remote Sensing of Environment. 2002. Vol. 81, № 2–3. P. 337–354.
doi: 10.1016/S0034-4257(02)00010-X

33. Strong L. L., Gilmer D. S., Brass J. A. Inventory of Wintering Geese with a Multispectral Scanner // J. of Wildlife Management. 1991. Vol. 55, № 2. P. 250–259.

34. Liu C. C., Chen Y. H., Wen H. L. Supporting the annual international black-faced spoonbill census with a low-cost unmanned aerial vehicle // Ecological Informatics. 2015. Vol. 30. P. 170–178.
doi: 10.1016/j.ecoinf.2015.10.008

35. O'Neill C. J., Roberts J. J., Cozzolino D. Identification of beef cattle categories (cows and calves) and sex based on the near infrared reflectance spectroscopy of their tail hair // Biosystems Engineering. 2017. Vol. 162. P. 140–146.
doi: 10.1016/j.biosystemseng.2017.07.007

36. Terletzky P., Ramsey R. D., Neale C. M. U. Spectral characteristics of domestic and wild mammals // GIScience & Remote Sensing. 2012. Vol. 49, № 4. P. 597–608.
doi: 10.2747/1548-1603.49.4.597

37. Trivedi M. M., Wyatt C. L., Anderson D. R. A multispectral approach to remote detection of deer. Photogramm // Eng. Remote Sens. 1982. Vol. 48, № 12. P. 1879–1889.

38. Spotting East African mammals in open savannah from space / Z. Yang, T. Wang, A. K. Skidmore, J. De Leeuw, M. Y. Said, J. Freer // PloS one. 2014. Vol. 9, № 12. P. e115989.
doi: 10.1371/journal.pone.0115989

39. Platonov N. G., Mordvintsev I. N., Rozhnov V. V. The possibility of using high resolution satellite images for detection of marine mammals // Biology Bulletin. 2013. Vol. 40. P. 197–205.
doi: 10.1134/S1062359013020106

40. Whales from space: four mysticete species described using new VHR satellite imagery / H. C. Cubaynes, P. T. Fretwell, C. Bamford, L. Gerrish, J. A. Jackson // Marine Mammal Science. 2019. Vol. 35, № 2. P. 466–491.
doi: 10.1111/mms.12544

41. Satellite imagery can be used to detect variation in abundance of Weddell seals (Leptonychotes weddellii) in Erebus Bay, Antarctica / M. A. LaRue, J. J. Rotella, R. A. Garrott, D. B. Siniff, D. G. Ainley, G. E. Stauffer, C. C. Porter, P. J. Morin // Polar Biology. 2011. Vol. 34. P. 1727–1737.
doi: 10.1007/s00300-011-1023-0

42. Applicability of Green-Red Vegetation Index for Remote Sensing of Vegetation Phenology / T. Motohka, K. N. Nasahara, H. Oguma, S. Tsuchida // Remote Sens. 2010. Vol. 2. P. 2369–2387.
doi: 10.3390/rs2102369

Информация об авторах

Горяинов Виктор Сергеевич – кандидат технических наук (2019), доцент кафедры фотоники Санкт-Петербургского государственного электротехнического университета "ЛЭТИ" им. В. И. Ульянова (Ленина). Автор более 40 научных работ. Сфера научных интересов – дистанционное зондирование Земли; спектрофотометрия; поляриметрия; лидары; оптика природных вод.
Адрес: Санкт-Петербургский государственный электротехнический университет "ЛЭТИ" им. В. И. Ульянова (Ленина), ул. Профессора Попова, д. 5 Ф, Санкт-Петербург, 197022, Россия
E-mail: vsgoriainov@etu.ru
https://orcid.org/0000-0003-2864-8717

Нгуа Ндонг Авеле Жак Бернис – магистр по направлению "Квантовая и оптическая электроника" (2024, Санкт-Петербургский государственный электротехнический университет "ЛЭТИ" им. В. И. Ульянова (Ленина)), аспирант кафедры радиотехнических систем Санкт-Петербургского государственного электротехнического университета "ЛЭТИ" им. В. И. Ульянова (Ленина). Автор шести научных публикаций. Сфера научных интересов – дистанционное зондирование Земли; спектрофотометрия; лидары; беспилотные летательные аппараты; машинное обучение.
Адрес: Санкт-Петербургский государственный электротехнический университет "ЛЭТИ" им. В. И. Ульянова (Ленина), ул. Профессора Попова, д. 5 Ф, Санкт-Петербург, 197022, Россия
E-mail: avelejacques@yahoo.fr
https://orcid.org/0009-0004-6564-0743

Мазоя Адам Бенджамин – окончил аспирантуру Санкт-Петербургского государственного электротехнического университета "ЛЭТИ" им. В. И. Ульянова (Ленина) по специальности "Оптические и оптико-электронные

приборы и комплексы" (2023), доцент кафедры электроники и телекоммуникаций Университета Додомы (UDOM), Танзания. Автор трех научных публикаций. Сфера научных интересов – дистанционное зондирование Земли; спектрофотометрия; беспилотные летательные аппараты; охраняемые природные территории.
Адрес: Университет Додомы, ул. Бенджамина Мкапы, д. 1, Ийумбу, Додома, 41218, Танзания.
E-mail: mazoya19@gmail.com
http://orcid.org/0009-0008-8658-1956

Тарасов Сергей Анатольевич – доктор технических наук (2016), заведующий кафедрой фотоники Санкт-Петербургского государственного электротехнического университета "ЛЭТИ" им. В. И. Ульянова (Ленина). Автор более 180 научных работ. Сфера научных интересов – агрофотоника; солнечная энергетика; физика и оптика полупроводников; светоизлучающие и фоточувствительные приборы.
Адрес: Санкт-Петербургский государственный электротехнический университет "ЛЭТИ" им. В. И. Ульянова (Ленина), ул. Профессора Попова, д. 5 Ф, Санкт-Петербург, 197022, Россия
E-mail: satarasov@mail.ru
http://orcid.org/0000-0002-6321-0019

References

1. Krinov E. L. Spectral Reflectance Properties of Natural Formations. Ottawa, National research council of Canada, 1953, 268 p.

2. Buznikov A. A. Space Spectrophotometry of The Natural Environment from Manned Orbital Stations. J. of Optical Technology. 2015, vol. 82, no. 7, pp. 487–493. doi: 10.1364/JOT.82.000487

3. Goryainov V. S., Buznikov A. A., Kostikov E. V. Redesigning the Portable RSS Spectrometer. Proc. of Saint Petersburg Electrotechnical University. 2020, no. 2, pp. 5–16. (In Russ.)

4. Raizer V. Optical Remote Sensing of Ocean Hydrodynamics. Boca Raton, CRC Press, 2019, 296 p. doi: 10.1201/9781351119184

5. Barnett T. L., Juday R. D. Skylab S191 Visible-Infrared Spectrometer. Applied Optics. 1977, vol. 16, no. 4, pp. 967–972. doi: 10.1364/AO.16.000967

6. Goetz A. F. H., Srivastava V. Mineralogical Mapping in the Cuprite Mining District, Nevada. Proc. of the Airborne Imaging Spectrometer Data Anal. Workshop. Pasadena. Jet Propulsion Laboratory, 1985, pp. 22−31.

7. Goetz A. F. H. Three Decades of Hyperspectral Remote Sensing of the Earth: a Personal View. Remote Sensing of Environment. 2009, vol. 113, pp. S.5–S.16. doi: 10.1016/j.rse.2007.12.014

8. Vane G., Goetz A. F. H., Wellman J. B. Airborne Imaging Spectrometer: a New Tool for Remote Sensing. IEEE Trans. Geosci. Remote Sens. 1984, vol. GE-22, no. 6, pp. 546–549. doi: 10.1109/TGRS.1984.6499168

9. Middleton E. M., Campbell P. K. E., Ong L., Landis D. R., Zhang Q., Neigh C. S., Huemmrich K. F., Ungar S. G., Mandl D. J., Frye S. W., Ly V. T., Cappelaere P. G., Chien S. A., Franks S., Pollack N. H. Hyperion: the First Global Orbital Spectrometer, Earth Observing-1 (EO-1) Satellite (2000–2017). IEEE Intern. Geoscience and Remote Sensing Symp. (IGARSS), Fort Worth, 23–28 July 2017. IEEE, 2017, pp. 3039–3042. doi: 10.1109/IGARSS.2017.8127639

10. Qian S.-E. Hyperspectral Satellites, Evolution, and Development History. IEEE J. of Selected Topics in Applied Earth Observations and Remote Sensing. 2021, vol. 14, pp. 7032–7056. doi: 10.1109/JSTARS.2021.3090256

11. Benhadj I., Livens S., Esposito M., Vercruyssen N., Van Dijk C., Soukup M., Marchi A. Z., Maresi L. HyperScout-1 Inflight Calibration and Product Validation. Intern. J. of Remote Sensing. 2024, vol. 45, no. 7, pp. 2486–2517. doi: 10.1080/01431161.2024.2331979

12. Wang J., He Z., Shu R., Xu R., Chen K., Li C. Visible and Near-Infrared Imaging Spectrometer Aboard Chinese Chang'E 3 Spacecraft. Optical Payloads for Space Missions. Chichester, Wiley, 2016, pp. 121–139. doi: 10.1002/9781118945179.ch5

13. Praks J., Niemelä P., Näsilä A., Kestilä A., Jovanovic N., Riwanto B., Tikka T., Leppinen H., Vainio R., Janhunen P. Miniature Spectral Imager in-Orbit Demonstration Results from Aalto-1 Nanosatellite Mission. IEEE Intern. Geoscience and Remote Sensing Symp., Valencia, 22–27 July 2018. IEEE, 2018, pp. 1986–1989. doi: 10.1109/IGARSS.2018.8517658

14. Zhao X., Xiao Z., Kang Q., Li Q., Fang L. Overview of the Fourier Transform Hyperspectral Imager (HSI) Boarded on HJ-1A Satellite. IEEE Intern. Geoscience and Remote Sensing Symp., Honolulu, 25–30 July 2010. IEEE, 2010, pp. 4272–4274. doi: 10.1109/IGARSS.2010.5649250

15. Ngom N. M., Baratoux D., Bolay M., Dessertine A., Saley A. A., Baratoux L., Mbaye M., Faye G., Yao A. K., Kouamé K. J. Artisanal Exploitation of Mineral Resources: Remote Sensing Observations of Environmental Consequences, Social and Ethical Aspects. Surveys in Geophysics. 2023, vol. 44, pp. 225–247. doi: 10.1007/s10712-022-09740-1

16. Lammoglia S.-K., Akpa Y. L., Danumah J. H., Brou Y. L. A., Kassi J. N. High-Resolution Multispectral and RGB Dataset from UAV Surveys of Ten Cocoa Agroforestry Typologies in Côte d'Ivoire. Data in Brief. 2024, vol. 55, art. no. 110664. doi: 10.1016/j.dib.2024.110664

17. Belcore E., Piras M., Pezzoli A., Massazza G., Rosso M. Raspberry Pi 3 Multispectral Low-Cost Sensor for UAV Based Remote Sensing. Case Study in South-West Niger. ISPRS, 2019, vol. XLII-2/W13, pp. 207–214. doi: 10.5194/isprs-archives-XLII-2-W13-207-2019

18. Adão T., Hruška J., Pádua L., Bessa J., Peres E., Morais R., Sousa J. J. Hyperspectral Imaging: A Review on UAV-Based Sensors, Data Processing and Applications for Agriculture and Forestry. Remote Sens. 2017, vol. 9, no. 11, art. no. 1110.
doi: 10.3390/rs9111110

19. Jang G., Kim J., Yu J.-K., Kim H.-J., Kim Y.-H., Kim D.-W., Kim K.-H., Lee C., Chung Y. S. Review: Cost-Effective Unmanned Aerial Vehicle (UAV) Platform for Field Plant Breeding Application. Remote Sensing. 2020, vol. 12, no. 6, art. no. 998.
doi: 10.3390/rs12060998

20. Baranov P. S., Chirkunova A. A. Television Camera of the Visible and Near-Infrared Ranges. J. of the Russin Universities. Radioelectronics. 2015, vol. 4, pp. 47–56. (In Russ.)

21. Ovchinnikov A. V. Multispectral Camera with Sequential Formation of Images. J. of Radioelectronics. 2021, no. 5, pp. 1–11. (In Russ.)
doi: 10.30898/1684-1719.2021.5.6

22. Mazeh F., El Sahili J., Zaraket H. Low-Cost NDVI Platform for Land Operation: Passive and Active. IEEE Sensors Let. 2021, vol. 5, no. 10, art. no. 5500804.
doi: 10.1109/LSENS.2021.3112822

23. Morales A., Guerra R., Horstrand P., Diaz M., Jimenez A., Melian J., Lopez S., Lopez J. F. A Multispectral Camera Development: From the Prototype Assembly until Its Use in a UAV System. Sensors. 2020, vol. 20, art. no. 6129.
doi: 10.3390/s20216129

24. Monteiro F., Bexiga V., Chaves P., Godinho J., Henriques D., Melo-Pinto P., Nunes T., Piedade F., Pimenta N., Sustelo L., Fernandes A. M. Classification of Fish Species Using Multispectral Data from a Low-Cost Camera and Machine Learning. Remote Sensing. 2023, vol. 15, art. no. 3952.
doi: 10.3390/rs15163952

25. Lopez-Ruiz N., Granados-Ortega F., Carvajal M. A., Martinez-Olmos A. Portable Multispectral Imaging System Based on Raspberry Pi. Sensor Review. 2017, vol. 37, no. 3, pp. 322–329.
doi: 10.1108/SR-12-2016-0276

26. Noguera M., Millan B., Andújar J. M. New, Low-Cost, Hand-Held Multispectral Device for In-Field Fruit-Ripening Assessment. Agriculture. 2023, vol. 13, no. 1, p. 4.
doi: 10.3390/agriculture13010004

27. Shiddiq M., Herman H., Arief D. S., Fitra E., Husein I. R., Ningsih S. A. Wavelength Selection of Multispectral Imaging for Oil Palm Fresh Fruit Ripeness Classification. Applied Optics. 2022, vol. 61, no. 17, pp. 5289–5298.
doi: 10.1364/AO.450384

28. OmniVision. OV5647 datasheet. Preliminary specification. Available at: https://cdn.sparkfun.com/datasheets/Dev/RaspberryPi/ov5647_full.pdf (accessed: 09.06.2025).

29. Goryainov V. S., Buznikov A. A. A Study of the Influence of Copper Sulfate on the Spectral Properties of Common Buckwheat (Fagopyrum Esculentum). J. of Physics: Conf. Ser. 2021, vol. 2103, no. 1, art. no. 012155.
doi: 10.1088/1742-6596/2103/1/012155

30. Sonobe R., Wang Q. Assessing the Xanthophyll Cycle in Natural Beech Leaves with Hyperspectral Reflectance. Functional Plant Biology. 2016, vol. 43, no. 5, pp. 438–447.
doi: 10.1071/FP15325

31. Gitelson A. A., Zur Y., Chivkunova O. B., Merzlyak M. N. Assessing Carotenoid Content in Plant Leaves with Reflectance Spectroscopy. Photochem. Photobiol. 2002, vol. 75, no. 3, pp. 272–281.
doi: 10.1562/0031-8655(2002)0750272ACCIPL2.0.CO2

32. Sims D. A., Gamon J. A. Relationships Between Leaf Pigment Content and Spectral Reflectance Across a Wide Range of Species, Leaf Structures and Developmental Stages. Remote Sensing of Environment. 2002, vol. 81, no. 2–3, pp. 337–354.
doi: 10.1016/S0034-4257(02)00010-X

33. Strong L. L., Gilmer D. S., Brass J. A. Inventory of Wintering Geese with a Multispectral Scanner. J. of Wildlife Management. 1991, vol. 55, no. 2, pp. 250–259.

34. Liu C. C., Chen Y. H., Wen H. L. Supporting the Annual International Black-Faced Spoonbill Census with a Low-Cost Unmanned Aerial Vehicle. Ecological Informatics. 2015, vol. 30, pp. 170–178.
doi: 10.1016/j.ecoinf.2015.10.008

35. O'Neill C. J., Roberts J. J., Cozzolino D. Identification of Beef Cattle Categories (Cows and Calves) and Sex Based on the Near Infrared Reflectance Spectroscopy of Their Tail Hair. Biosystems Engineering. 2017, vol. 162, pp. 140–146.
doi: 10.1016/j.biosystemseng.2017.07.007

36. Terletzky P., Ramsey R. D., Neale C. M. U. Spectral Characteristics of Domestic and Wild Mammals. GIScience & Remote Sensing. 2012, vol. 49, no. 4, pp. 597–608.
doi: 10.2747/1548-1603.49.4.597

37. Trivedi M. M., Wyatt C. L., Anderson D. R. A Multispectral Approach to Remote Detection of Deer. Photogramm. Eng. Remote Sens. 1982, vol. 48, no. 12, pp. 1879–1889.

38. Yang Z., Wang T., Skidmore A. K., De Leeuw J., Said M. Y., Freer J. Spotting East African Mammals in Open Savannah from Space. PloS One. 2014, vol. 9, no. 12, p. e115989.
doi: 10.1371/journal.pone.0115989

39. Platonov N. G., Mordvintsev I. N., Rozhnov V. V. The Possibility of Using High Resolution Satellite Images for Detection of Marine Mammals. Biology Bulletin. 2013, vol. 40, pp. 197–205.
doi: 10.1134/S1062359013020106

40. Cubaynes H. C., Fretwell P. T., Bamford C., Gerrish L., Jackson J. A. Whales from Space: Four Mysticete Species Described Using New VHR Satellite Imagery. Marine Mammal Science. 2019, vol. 35, no. 2, pp. 466–491.
doi: 10.1111/mms.12544

41. LaRue M. A., Rotella J. J., Garrott R. A., Siniff D. B., Ainley D. G., Stauffer G. E., Porter C. C., Morin P. J. Satellite Imagery Can Be Used to Detect Variation in Abun-

dance of Weddell Seals (Leptonychotes Weddellii) in Erebus Bay, Antarctica. Polar Biology. 2011, vol. 34, pp. 1727–1737.
doi: 10.1007/s00300-011-1023-0

42. Motohka T., Nasahara K. N., Oguma H., Tsuchida S. Applicability of Green-Red Vegetation Index for Remote Sensing of Vegetation Phenology. Remote Sens. 2010, vol. 2, pp. 2369–2387.
doi: 10.3390/rs2102369

Information about the authors

Viktor S. Goryainov, Cand. Sci. (Eng.) (2019), Associate Professor of the Department of Photonics of Saint Petersburg Electrotechnical University. The author of more than 40 scientific publications. Area of expertise: remote sensing of the Earth; spectrophotometry; polarimetry; lidars; optics of natural waters.
Address: Saint Petersburg Electrotechnical University, 5F, Professor Popov St., St Petersburg 197022, Russia
E-mail: vsgoriainov@etu.ru
https://orcid.org/0000-0003-2864-8717

Jacques B. Ngoua Ndong Avele, Master in quantum and optical electronics (2019, Saint Petersburg Electrotechnical University), Postgraduate student of the Department of Radiotechnical Systems of Saint Petersburg Electrotechnical University. The author of 6 scientific publications. Area of expertise: remote sensing of the Earth; spectrophotometry; lidars; unmanned aerial vehicles; machine learning.
Address: Saint Petersburg Electrotechnical University, 5F, Professor Popov St., St Petersburg 197022, Russia
E-mail: avelejacques@yahoo.fr
https://orcid.org/0009-0004-6564-0743

Adam B. Mazoya, Postgraduate studies in optical and optoelectronic devices and complexes in Saint Petersburg Electrotechnical University (2023), Associate Professor of the Department of Electronics and Telecommunications of University of Dodoma (UDOM), Tanzania. The author of 3 scientific publications. Area of expertise: remote sensing of the Earth; spectrophotometry; unmanned aerial vehicles; protected areas.
Address: University of Dodoma, Benjamin Mkapa rd., 1, Iyumbu, Dodoma 41218, Tanzania
E-mail: mazoya19@gmail.com
http://orcid.org/0009-0008-8658-1956

Sergey A. Tarasov, Dr Sci. (Eng.) (2016), Head of the Department of Photonics of Saint Petersburg Electrotechnical University. The author of more than 180 scientific publications. Area of expertise: agrophotonics; solar energy; physics and optics of semiconductors; light-emitting and photosensitive materials.
Address: Saint Petersburg Electrotechnical University, 5F, Professor Popov St., St Petersburg 197022, Russia
E-mail: satarasov@mail.ru
http://orcid.org/0000-0002-6321-0019